SCIENTIFIC REPORTS

natureresearch

Check for updates

OPEN

Time-dependent branching processes: a model of oscillating neuronal avalanches

Johannes Pausch[1,2✉], Rosalba Garcia-Millan[2] & Gunnar Pruessner[2]

Recently, neuronal avalanches have been observed to display oscillations, a phenomenon regarded as the co-existence of a scale-free behaviour (the avalanches close to criticality) and scale-dependent dynamics (the oscillations). Ordinary continuous-time branching processes with constant extinction and branching rates are commonly used as models of neuronal activity, yet they lack any such time-dependence. In the present work, we extend a basic branching process by allowing the extinction rate to oscillate in time as a new model to describe cortical dynamics. By means of a perturbative field theory, we derive relevant observables in closed form. We support our findings by quantitative comparison to numerics and qualitative comparison to available experimental results.

In the brain, electrical signals propagate between neurons of the cortical network through action potentials, which are spikes of polarisation in the membrane of the neuron's axon. These spikes have an amplitude of about 100 mV, typically last about 1 ms[1] and can be recorded using micro-electrodes[2,3]. In order to study the signaling in larger regions of neurons, multielectrode arrays, comprising about 60 electrodes spread across $\approx 4\,\text{mm}^2$, are used to capture the collective occurrence of spikes as local field potentials (LFPs). In this setting, the electrodes are extracellular and each is sensitive to electrical signals from several surrounding neurons[4–8].

The data of the LFP recordings are processed by putting them into time bins of a few milliseconds duration and by introducing a voltage threshold. In addition, a refractory period is imposed to avoid counting large voltage excursions more than once.

The details of processing can differ slightly between experiments[5–9]. However, after processing, the data is a time series of two values for each electrode: on (detected signal above threshold) and off (no detected signal or signal below threshold). A *neuronal avalanche* is then defined as a set of uninterrupted signals detected across the micro-electrode array. Each avalanche is both preceded and succeeded by at least one time bin where none of the electrodes detected a signal, defining the avalanche duration as the number of time bins where the avalanche unfolds. Which and how many electrodes detect a signal varies during the avalanche[5,6]. The duration of avalanches typically ranges between a few milliseconds and 30 ms[10]. A prominent observable is the avalanche size, which is the total number of recorded signals during the avalanche. If there is only one electrode detecting a signal in each time bin of an avalanche, its size and duration are equal. However, the size of an avalanche is usually larger than its duration due to the simultaneous detection of signals by different electrodes. Histograms of the avalanche size show an apparent *power-law distribution of sizes*, with common small avalanches and rare large avalanches[5,6], the fingerprint of scale-free phenomena. The exponent of the power law was observed to be $-3/2$ in Ref.[5]. However, its exact value was found to be significantly sensitive to the choice of time bin size[8] and spatial sub-sampling of the neural network[7].

The observation of this power-law distribution led to the hypothesis that neuronal avalanches can be modelled adequately by models in the class of self-organized-criticality (SOC)[5,8,11] or models of critical branching processes[5,12–14], because both are avalanche models showing power-law distribution of the avalanche size[15,16]. In this article, we focus on modelling neuronal avalanches as branching processes.

A *branching process* is a stochastic process in which a particle can either randomly create identical copies of itself or spontaneously go extinct, triggering an avalanche of particles[16–21, 21–27]. The particle number N in the branching process is interpreted as the number of electrodes that detect a signal. The creation of a new particle is interpreted as the change of an electrode from no detection to the detection of a signal[5], while the extinction

---

[1]Department of Applied Mathematics and Theoretical Physics and St. Catharine's College, University of Cambridge, Cambridge CB3 0WA, UK. [2]Department of Mathematics and Centre for Complexity Science, Imperial College London, London SW7 2AZ, UK. ✉email: jp634@cam.ac.uk

of a particle corresponds to the change from detection to no detection[8,14,28]. Branching processes display a phase transition from asymptotic extinction with probability 1 to asymptotic survival with a positive probability, depending on the average number of created particles. At the critical point, the avalanche size of a branching process is power-law distributed[16].

Recently, there has been evidence that neuronal activity, when compared to branching processes, is not at criticality but in a reverberating regime close to criticality[14,29,30]. The reason for the strong interest in the system's distance to a critical point is the criticality hypothesis, which states that information processing in the brain might be optimized by the cortical network being close to a critical point[10,12,13,31,32]. However, fitting power laws is notoriously difficult[30,33] and other means of verifying the criticality of the neuronal avalanches are essential. For this reason, the *avalanche shape*, defined as the average temporal profile of the avalanches, has received more attention in recent years. It is debated whether, at criticality, the neuronal avalanche shape takes the universal form of an inverse parabola[16,26,34–38], which is the case of a critical branching process. The universality of this shape has been particularly challenged in Ref.[38] by observations of oscillations that modulate the avalanche shape. In Ref.[38], the oscillations are identified as γ-oscillations, which are a particular frequency band of brain waves between 30 and 100 Hz. Brain waves are electric oscillations spanning the entire brain that can be recorded using electroencephalography (EEG)[39,40]. The oscillations are organized into bands covering frequencies between 0.05 Hz (slow 4 band) and 500 Hz (ultra fast band). Their power spectrum follows approximately a $1/f$ distribution[41]. Statistically, they are linked to the quiet time distribution between avalanches and correlations between avalanche sizes[42]. Their physiological role and the biological mechanisms that sustain them continue to attract attention in neuroscience[43–48].

The observation of oscillations in the EEG activity on the one hand, and the observation of scale-free avalanches of LFP activity on the other hand raises the question of how these two seemingly incompatible descriptions of the same phenomena can be reconciled. The experimental data in Ref.[38] indicates that γ-oscillations modulate the avalanche shape. Can branching processes incorporate oscillations as well? Will those oscillations modulate the avalanche shape, widely regarded as a universal feature?

To answer these questions, we extend in this paper the field theory in Ref.[16] by incorporating oscillatory extinction rates, see "Model". We then calculate observables such as "Moments" of the particles number, its "Covariance", "Survival probability", and the "Avalanche shape" (or temporal profile) and compare them qualitatively to experimental results from Ref.[38]. We conclude in "Discussion and conclusion".

Model

A branching process in continuous time t can be regarded as a reaction of a single particle type B that splits into $K \in \mathbb{N}_0$ copies of itself,

$$B \xrightarrow{s} KB, \tag{1}$$

with Poissonian rate s[18–20]. The particle number at time t, which is also called population size, is denoted by $N(t)$. In the event of a reaction, the population size increases by $K - 1$ particles. The waiting time for an individual particle to undergo any such reaction is exponentially distributed with rate s. The number of offspring K may be a random variable itself, with probability distribution $P(K = k) = p_k$. We call the reaction in (1) a branching event if $K > 1$ and an extinction event if $K = 0$. Throughout the present work we initialize the process with one particle at time $t_0 = 0$, so that $N(0) = 1$. The totality of a realisation of a branching process, from the initialization until the termination after which the population size remains 0 indefinitely is referred to as an avalanche. Times between avalanches are not modelled[49] and there are no correlations between avalanches[42].

In Ref.[16], we introduced a Doi–Peliti field theory for the continuous-time branching process with time-independent but arbitrary offspring distribution p_k. We refer to such a branching process as *standard branching process*. The action functional of this field theory is

$$\mathcal{A}_0[\phi, \widetilde{\phi}] = \int \left\{ \widetilde{\phi}\left(-\frac{d}{dt} - r\right)\phi + \sum_{j=2}^{\infty} q_j \widetilde{\phi}^j \phi \right\} dt, \tag{2}$$
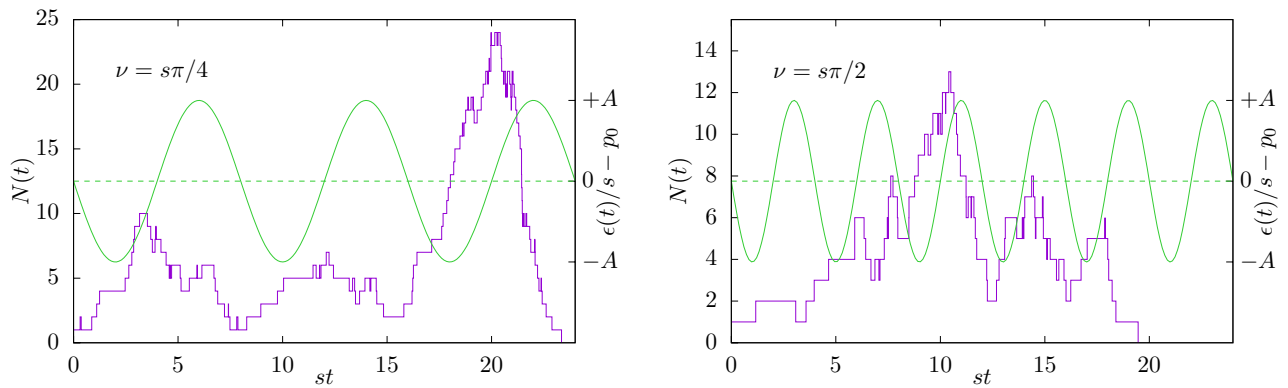
with

$$r = s(1 - \mathbb{E}[K]) \text{ and } q_j = s\sum_{k=j}^{\infty} \binom{k}{j} p_k, \tag{3}$$

and time-dependent Doi-shifted annihilation and creation fields $\phi(t)$ and $\widetilde{\phi}(t)$ respectively. The parameter r is called the mass in the context of field theories and is, according to Eq. (3), closely linked to the first moment of the offspring distribution $\mathbb{E}[K]$. Traditionally[18], the branching process is called *sub-critical* if $\mathbb{E}[K] < 1$ (and thus $r > 0$), it is called *critical* if $\mathbb{E}[K] = 1$ (and thus $r = 0$), and *super-critical* if $\mathbb{E}[K] > 1$ (and thus $r < 0$).

The time-scale of this branching process is set by s, the rate with which *any* single-particle event takes place. The rate with which any particle spontaneously disappears, the extinction rate, is thus $\epsilon = sp_0$.

In the following we will focus on binary branching processes, i.e. $p_k = 0$ for all k except $k = 0$ and $k = 2$, so that p_2 and $p_0 = 1 - p_2$ in Eq. (3) are determined by $r/s = 1 - 2p_2$. The rest of parameters follow then immediately, such as $\mathbb{E}[K] = 2p_2$, $q_2/s = p_2 = 1/2(1 - r/s)$ and $q_j = 0$ for $j \geq 3$, as well as bounds such as $s \geq r + q_2 \geq 0$. In particular $r = \epsilon - q_2$, so that the branching process is critical if q_2 balances the extinction rate. Extensions to branching processes with other time-independent offspring distributions are straight forward[16].

Our extension to this model (2) consists of a *time-dependent*, oscillating extinction rate

Figure 1. Two example trajectories of the number of particles $N(t)$ (purple, left ordinate) of branching processes with $r = 0$ and periodically varying extinction rate $\epsilon(t) = s(p_0 - A\sin(\nu t))$, Eq. (4). Both trajectories were initialized with one particle at $t_0 = 0$. The perturbation of the extinction rate, $-A\sin(\nu t)$ with $\nu/s \in \{\pi/4, \pi/2\}$, $A = 0.5$ is shown in green (right ordinate). When the extinction rate is lower, branching is effectively promoted.

$$\epsilon(t) = s\big(p_0 - A\sin(\nu t)\big), \tag{4}$$

where ν is the frequency of the oscillations. The dimensionless amplitude A is the small parameter of the field theoretic perturbation theory about $A = 0$. Our model takes the oscillations as given and for simplicity idealizes them as sinus functions[50]. It does not model their emergence from underlying mechanisms. In the following, $r \geq 0$ is considered. The magnitude $|A|$ is bounded by p_0 because $\epsilon(t)$, as an extinction rate, has to be non-negative at all times. If the amplitude A is positive, then the extinction rate is initially suppressed, favouring more branching events. In the field theory, this extension amounts to adding the term (details in "Extension of the action"),

$$As \int \left\{ \widetilde{\phi}(t)\phi(t)\sin(\nu t) \right\} \mathrm{d}t, \tag{5}$$

to the original action $\mathcal{A}_0$, Eq. (2), where $r = sp_0 - sp_2$ is still the "bare mass". Our extension can be summarised as a standard branching process where binary branching takes place with rate $q_2 = sp_2$ and extinction with rate $\epsilon(t)$, Eq. (4). We retain the parameterisation $p_0 + p_2 = 1$.

It will turn out that the perturbation remains noticeable at all times in the process in all observables considered. In particular, even at criticality, the "Avalanche shape" carries a clear signature of the oscillations despite its expected universality[34]. The model and the analysis in the present work therefore provide an explanation for the shape of the temporal profile of neuronal avalanches recently reported by Miller et al.[38].

Figure 1 shows two example trajectories of the population size $N(t)$, together with the perturbation of the extinction rate, $\epsilon(t)/s - p_0 = -A\sin(\nu t)$. In all figures, the latter is shown in green with the ordinate on the right. All data in this work is presented in dimensionless form, in particular time as st.

In the following, we state the central results, whose field-theoretic derivation is relegated to the Appendix. In particular, we consider the "Avalanche shape" at criticality, which is a common observable in LFP recordings of the brain[5–8] and the "Covariance", which recently gained more attention in neuroscience as a tool to estimate the system's distance to the critical point[14,29,30].
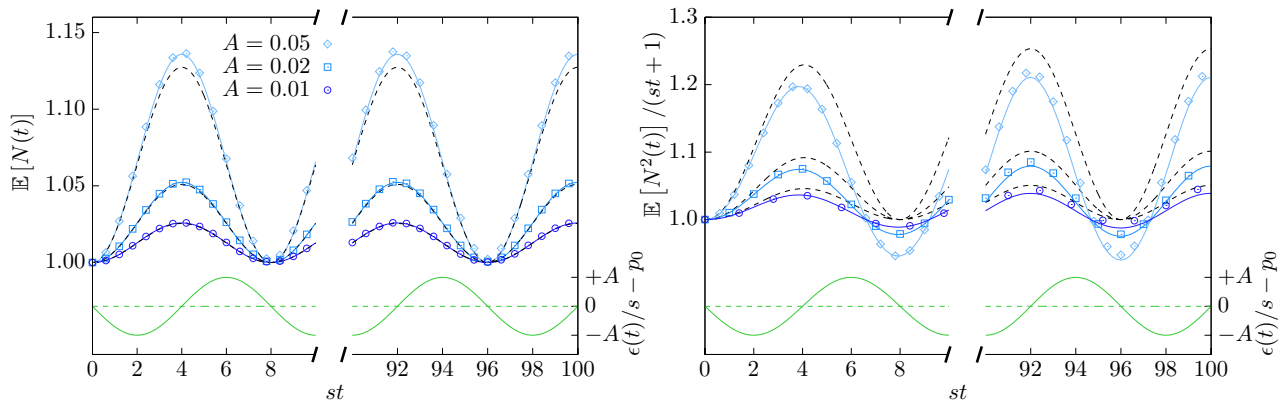
Moments

First moment. Since the extinction rate varies periodically, we expect that the first moment varies accordingly. As shown in "Appendix: First moment", the expected particle number is,

$$\mathbb{E}[N(t)] = \Theta(t)\exp\left(-rt + \int_0^t As\sin(\nu t')\mathrm{d}t'\right) = \Theta(t)\exp\left(-rt - \frac{As}{\nu}(\cos(\nu t) - 1)\right), \tag{6}$$

where $\Theta(t)$ is the Heaviside function reflecting the initialization at $t_0 = 0$, henceforth dropped from all expressions. This result is consistent with the known result of an inhomogenous Poisson process with a time-dependent event rate[51].

Figure 2 shows an estimate of the first moment based on Monte-Carlo simulations together with the analytical result Eq. (6) for $r = 0$. In addition to this exact result, the dashed line in Fig. 2 shows the first order approximation $\mathbb{E}[N(t)] = g_1^{(0)}(0, t) + Ag_1^{(1)}(0, t) + \mathcal{O}(A^2)$, Eq. (10), which is discussed below in "n-th factorial moment to first order".

Because the extinction rate is reduced during the first half-period, Eq. (4), branching dominates the process and the population size increases at first. During the second half-period, extinction dominates and the population size decreases, perfectly balancing, on average, the creation of particles in the first half of the period. According to Eq. (6) and Fig. 2, the expected population size $\mathbb{E}[N(t)]$ at $r = 0$ is always equal or larger than unity, which is

Figure 2. First and second moment of particle number for $A \in \{0.01, 0.02, 0.05\}$, $\nu/s = \pi/4$ and $r = 0$. The system was initialized with a single particle at $t_0 = 0$. Symbols: simulation results. Left: first moment (10^9 realizations). Right: rescaled second moment (10^7 realizations). Full blue lines: exact analytic predictions, Eq. (6) (left), Eq. (7) (right). Dashed black lines: analytic approximation, see Eqs. (10), (12), (16a), and (16b). The perturbation of the extinction rate, Eq. (4), is shown in green (right ordinate).

the expected number of particles of a standard branching process at criticality. Thus, while the extinction rate is not shifted on average, the expected particle number is on average larger than in the process without oscillations.

Just like in a standard branching process, $\mathbb{E}[N(t)]$ converges to 0 for $r > 0$ and diverges for $r < 0$, indicating that the present process is critical at $r = 0$. However, unlike a standard branching process, the expected population size never converges for $r = 0$ as the oscillations never cease. It will turn out that the effective mass acquires no shift due to the perturbation.

Second moment. The second moment can be calculated in closed form from a convolution integral involving the first moment only, "Appendix: Second moment". From Eqs. (32b), (33) and (35),

$$\mathbb{E}[N^2(t)] = \exp\left(-rt - \frac{As}{\nu}\big(\cos(\nu t) - 1\big)\right)\left[1 + 2q_2 \int_0^t \exp\left(-r(t - t') - \frac{As}{\nu}\big(\cos(\nu t) - \cos(\nu t')\big)\right)\mathrm{d}t'\right].$$

(7)

At $r = 0$ the second moment is, to first order in A,

$$\mathbb{E}[N^2(t)] = 1 + 2q_2 t + \frac{As}{\nu}\left[1 + 2q_2 t + \frac{2q_2}{\nu}\sin(\nu t) - (1 + 4q_2 t)\cos(\nu t)\right] + \mathcal{O}\big(A^2\big),$$

(8)

which diverges asymptotically linear in t. Because $\mathbb{E}[N(t)]$ is bounded, the variance also diverges linearly in t. Figure 2 shows the ratio $\mathbb{E}[N^2(t)]/(1 + 2q_2 t)$, which illustrates the deviation of the second moment at $A > 0$ from that at $A = 0$. For large t, the second moment shows a linear increase with an amplitude that oscillates mildly with period ν, so that $\mathbb{E}[N^2(t)]$ oscillates around the $A = 0$ behaviour. For large $q_2 t$ the ratio $\mathbb{E}[N^2(t)]/(1 + 2q_2 t)$ is to leading order $1 - (As/\nu)(2\cos(\nu t) - 1)$.

Although the extinction is not shifted on average, the second moment is shifted on average due to the oscillations, see Fig. 2.

n-th moment. In principle, all moments of $N(t)$ can be calculated exactly, following the same lines as in the previous section "Second moment" and in "Appendix: Second moment". However, even the second moment involves an integral that cannot be carried out in closed form and, for higher moments, the procedure quickly becomes unpleasantly complicated. To calculate higher moments of the population size $\mathbb{E}[N^n(t)]$, we resort to a perturbative expansion in powers of the amplitude A, which can be systematically expressed in terms of diagrams shown in the appendix.

Following[16], all moments can be written in terms of factorial moments, which are naturally produced by the diagrammatics of the field theory. We denote the n-th factorial moment by $g_n(t_0, t)$, so that

$$\mathbb{E}[N^n(t)|N(t_0) = 1] = \sum_{\ell=0}^n \begin{Bmatrix} n \\ \ell \end{Bmatrix} g_\ell(t_0, t),$$

(9)

where $\begin{Bmatrix} n \\ \ell \end{Bmatrix}$ are the Stirling numbers of the second kind. In the following, the factorial moments are expressed in orders of A,

$$g_n(t_0, t) = g_n^{(0)}(t_0, t) + A g_n^{(1)}(t_0, t) + \mathcal{O}(A^2).$$

(10)

The n-th factorial moment at $A = 0$, given by

$$g_n^{(0)}(t_0, t) = n! e^{-r(t-t_0)} \left(\frac{q_2}{r} \left(1 - e^{-r(t-t_0)} \right) \right)^{n-1}, \tag{11}$$

was calculated in closed form from the diagrams as a matter of combinatorics[16]. The function $g_n^{(0)}$ is dominated by $(q_2(t-t_0))^{n-1}$ for small $r(t-t_0) \ll 1$, while it is exponentially decaying for large $r(t-t_0) \gg 1$. In the present work, the factorial moments acquire a dependence on the initial time t_0, when $N(t_0) = 1$. Only to zeroth order in A, at $A = 0$, do the factorial moments become time-homogeneous and reduce to those calculated in Ref.[16], $g_n^{(0)}(t_0, t) = g_n^{(0)}(0, t - t_0)$. The next order term in the small-A expansion equals

$$g_n^{(1)}(t_0, t) = g_n^{(0)}(t_0, t) s \int_0^{t-t_0} \sin(\nu(t - t')) \left(1 + (n-1) \frac{e^{-rt'} - e^{-r(t-t_0)}}{1 - e^{-r(t-t_0)}} \right) dt', \tag{12}$$

whose derivation is explained in "Appendix: n-th factorial moment to first order".

In the subcritical regime $r > 0$, in large $r(t - t_0) \gg 1$ all moments vanish exponentially, because $g_n^{(0)}$ vanishes exponentially, see Eq. (11). For small $r(t - t_0) \ll 1$ and large $q_2(t - t_0) \gg 1$, the moments are dominated by the largest factorial moment,

$$\text{for } rt \ll 1: \quad \lim_{t \to \infty} \frac{\mathbb{E}[N^n(t)]}{g_n(0, t)} = 1. \tag{13}$$

This can be seen by expanding $\mathbb{E}[N^n(t)]$ in terms of the factorial moments which are asymptotically dominated by $g_n(t_0, t) \sim \mathcal{O}((q_2 t)^{n-1})$,

$$\mathbb{E}[N^n(t)] = g_n(0, t) + \begin{Bmatrix} n \\ 2 \end{Bmatrix} \underbrace{g_{n-1}(0, t)}_{\sim \mathcal{O}((q_2 t)^{n-2})} + \cdots \tag{14}$$

Within the small-A expansion of the n-th factorial moment, the terms $g_n^{(0)}$ and $g_n^{(1)}$ dominate $\mathbb{E}[N^n(t)]$, such that

$$\mathbb{E}[N^n(t)] = g_n^{(0)}(0, t) + A g_n^{(1)}(0, t) + \mathcal{O}\left(A^2 (q_2 t)^{n-1} \right) + \mathcal{O}\left((q_2 t)^{n-2} \right). \tag{15}$$

However, from Eq. (12) it can be seen that the oscillations in the amplitude of $g_n^{(0)}(t_0, t)$ in $g_n^{(1)}(t_0, t)$ will never cease, so that the limit $\lim_{t \to \infty} \mathbb{E}[N^n(t)]/(q_2(t - t_0))^{n-1}$ strictly does not exist. In other words, $g_n(t_0, t)$ captures the leading order of $\mathbb{E}[N^n(t)]$ in t, but $(q_2(t - t_0))^{n-1}$ does not.

The first two moments at $r = 0$ can be approximated to first order in A by

$$\mathbb{E}[N(t)] = 1 - \frac{As}{\nu}(\cos(\nu t) - 1) + \mathcal{O}(A^2), \tag{16a}$$

$$\mathbb{E}[N^2(t)] = 2q_2 t \left(1 + \frac{As}{\nu}(1 - 2\cos(\nu t)) + \mathcal{O}(A^2) \right) + \mathcal{O}\left((q_2 t)^0 \right), \tag{16b}$$

on the basis of Eqs. (12) and (15). The expressions are consistent with the exact expressions Eqs. (6) and (7) [as given in Eq. (8)], respectively. Figure 2 shows a comparison between the exact expressions (solid blue lines) and the approximation Eq. (16) (black dashed lines). Deviations are clearly noticeable only for large amplitudes A.

Further observables

In the following, we analyse observables that are somewhat more involved to derive in the present framework. In particular, the avalanche shape and covariance are more of immediate interest to experimentalists because these are more accessible from LFP recordings of the brain[5–8,14,29,30].

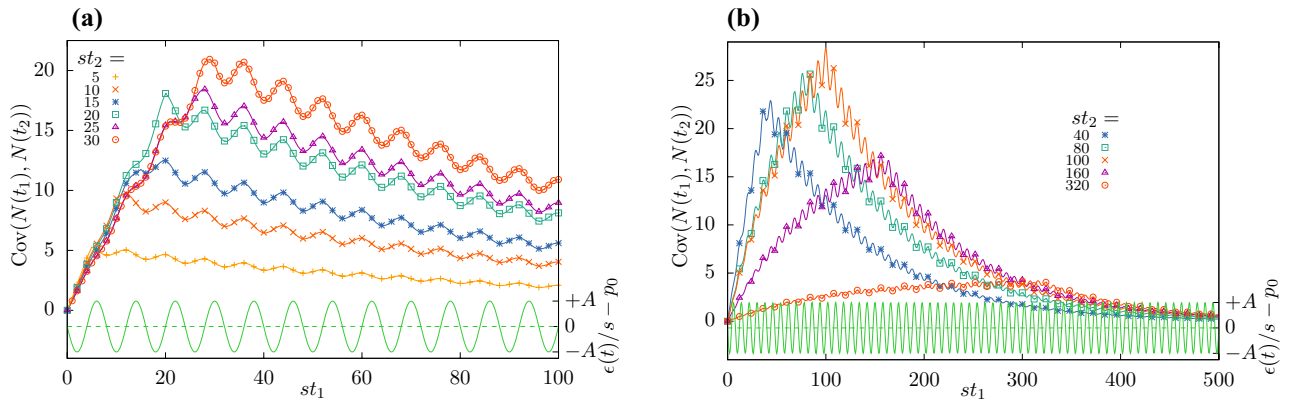**Covariance.** The autocorrelation function

$$\text{Cov}(N(t_1), N(t_2)) = \mathbb{E}[N(t_1)N(t_2)] - \mathbb{E}[N(t_1)]\mathbb{E}[N(t_2)] \tag{17}$$

is the covariance of $N(t_1)$ and $N(t_2)$ and it is a common way to quantify how strongly correlated data are at different points in time. If the population size at different times was independent, the autocorrelation function at times t_1 and t_2, $t_1 \neq t_2$, would be zero (the converse does not hold in general[52]).

As shown in "Appendix: Covariance", the covariance can be calculated in closed form up to an integral,

$$\text{Cov}(N(t_1), N(t_2)) = -\exp\left(-r(t_1 + t_2) + \frac{As}{\nu}(\cos(\nu t_1) + \cos(\nu t_2) - 2) \right)$$

$$+ \exp\left(-rt_{\max} + \frac{As}{\nu}(\cos(\nu t_{\max}) - 1) \right) \left[1 + 2q_2 \int_0^{t_{\min}} \exp\left(r(t' - t_{\min}) + \frac{As}{\nu}(\cos(\nu t_{\min}) - \cos(\nu t')) \right) dt' \right], \tag{18}$$

where $t_{\min} = \min\{t_1, t_2\}$ and $t_{\max} = \max\{t_1, t_2\}$.

Figure 3. Covariance $\text{Cov}(N(t_1), N(t_2))$ Eq. (17) for $r/s = 0.01$, $v/s = \pi/4$, $A = 0.05$ and (**a**) $st_2 = 5, 10, 15, \ldots, 30$, (**b**) $st_2 = 40, 80, 100, 160, 320$. The system was initialized with a single particle at time $t_0 = 0$. Symbols: simulations results from 10^9 trajectories. Full lines: analytic expression, Eq. (18). The perturbation of the extinction rate, Eq. (4), is shown in green at the bottom of the figure (right ordinate).

Simulation results and analytical expression Eq. (18) are shown together in Fig. 3a,b. For $A = 0$, the maximum of $\text{Cov}(N(t_1), N(t_2))$ occurs at $t_1 = t_2 = t$ and equals $(2q_2/r + 1)(\exp{-rt} - \exp{-2rt})$[16]. Furthermore, its maximum rises with increasing t, provided that $rt < \log(2)$. When $A \neq 0$, these results are only approximations and the exact position of the maximum depends on the phase and amplitude of the oscillations. In Fig. 3a, all st_2 are chosen to fulfil that condition, while in Fig. 3b, the larger st_2 don't meet this condition and show a decreasing maximum.

As an autocorrelation function, the covariance quantifies how the activity in the system at one instance influences the system at later instances. This has recently proven to be a valuable tool for determining the distance of neural networks from the critical point[14,29,30]. What the imposed oscillations imply for this tool is discussed in "Discussion and conclusion".

Survival probability. The "First moment" shows that the expected number of particles is on average larger if $A > 0$, i.e. if the extinction rate drops before growing in every period, compared to the case without oscillations or reversed order of rise and fall of extinction, $A < 0$. As noted in "First moment", the sign of the mass r still determines whether $\mathbb{E}[N(t)]$ ultimately vanishes or diverges, even when $\mathbb{E}[N(t)]$ oscillates indefinitely for $r = 0$. This observation raises the question whether the survival probability $P_s(t_0, t)$, that is the probability of $N(t) > 0$ at a given time t after initialization at t_0, displays a corresponding behaviour.

Based on the derivation in "Appendix: Probability of survival to first order", to leading order in A we find

$$\lim_{r \to 0} P_s(t_0 = 0, t) = \frac{1}{1 + q_2 t} + \frac{As}{v}\left(\frac{1}{1 + q_2 t} - \frac{\cos(vt) + \frac{q_2}{v}\sin(vt)}{(1 + q_2 t)^2}\right) + \mathcal{O}(A^2). \quad (19)$$

The first term, which is independent of A, is the probability of survival of the critical branching process with constant extinction rate[16] (Fig. 4). The second term is the first-order correction and indicates a shift of the probability of survival. For positive A (leading to an initial decrease of the extinction rate) the survival probability increases compared to the system without oscillations. For negative A (corresponding to an initial increase of the extinction rate) it decreases. For $A > 0$, the initial push into the supercritical phase seems to dominate the entire survival probability, even many oscillations later, see Fig. 4.

Despite the shifted survival probabilities, Fig. 4, and shifted average number of particles, Fig. 2, the avalanches do not survive indefinitely. They die eventually with probability 1 at $r = 0$. As the survival probability at criticality is shifted, Eq. (19), it can be expected that the avalanche duration distribution P_T is affected by the oscillations. Considering that the avalanche duration is equal to the time of death T of an avalanche that started at $t = 0$, it can be derived from the survival probability $P_T(t) = -\frac{dP_s(t)}{dt}$[16]:

$$\lim_{r \to 0} P_T(t) = \frac{q_2}{(1 + q_2 t)^2}\left(1 + \frac{As}{v}\right) + \frac{As}{v}\left(\frac{-v\sin(vt) + q_2\cos(vt)}{(1 + q_2 t)^2} - 2q_2\frac{\cos(vt) + \frac{q_2}{v}\sin(vt)}{(1 + q_2 t)^3}\right) + \mathcal{O}(A^2). \quad (20)$$

It shows that the distribution of durations still follows the $\sim t^{-2}$ power law of conventional critical branching with constant extinction rate[16], Fig. 5 (left panel). However, this power law has oscillations superimposed, which means that, strictly, scale invariance at criticality is broken. Yet, in a data-analysis based on binning the avalanche durations, these oscillations will be averaged out and thus not be visible. Similarly, simulations of the avalanche size distribution P_S show that for small oscillation amplitudes, the power law distribution with exponent $3/2$ appears to be maintained and the effect of oscillations is averaged out, Fig. 5 (right panel).

To appreciate better the effect of the extinction oscillations on the ultimate survival $\lim_{t \to \infty} P_s(t_0, t)$, we also consider the asymptotics of large t for $r > 0$ or equivalently $p_0 > p_2$,

6
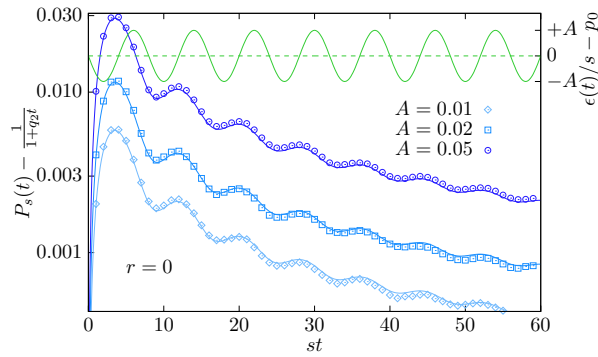
Figure 4. Difference between the probability of survival $P_s(0, t)$ at $r = 0$, Eq. (19) with and without oscillations, for $v/s = \pi/4$ and $A \in \{0.01, 0.02, 0.05\}$. The system was initialized with one particle at time $t_0 = 0$. Symbols: simulations results using 3×10^7 trajectories for $A = 0.01$ and 10^7 otherwise. Full blue lines: analytic prediction to first order in A. Full green lines: perturbation of the extinction rate, Eq. (4) (right ordinate).
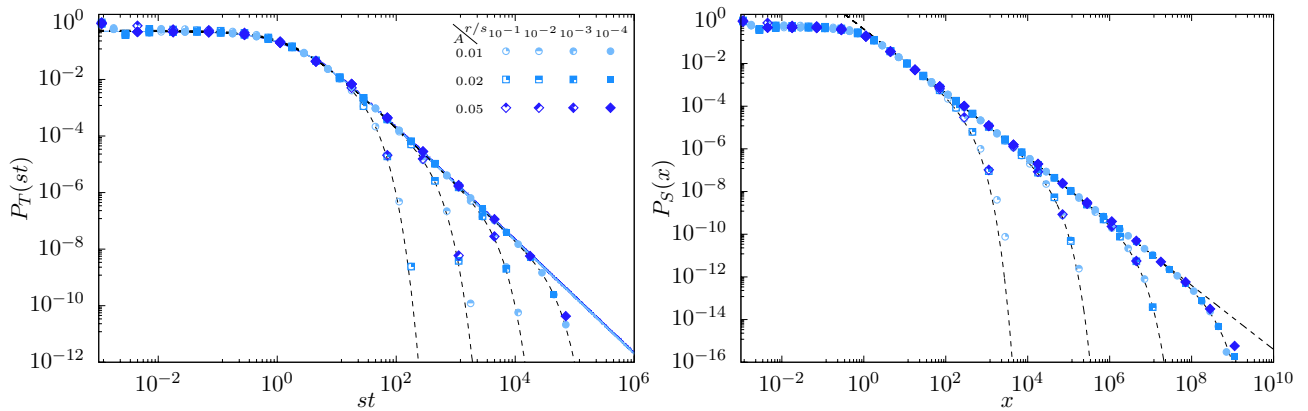
Figure 5. Probability density function of avalanche durations P_T (left) and sizes P_S (right). Symbols: simulations. Dashed lines: theoretical prediction without oscillations, Eq. (44) (left) and Eq. (63) (right) in Ref.[16]. Blue solid lines (left only): theoretical prediction with oscillation at criticality, Eq. (20).

$$\text{for } rt \gg 1 \quad P_s(0, t)|_{r>0} \simeq \frac{\exp -rt}{1 + q_2/r}\left(1 + \frac{As}{v}(1 - \cos(vt)) + \mathcal{O}(A^2)\right) \xrightarrow{t \to \infty} 0 \tag{21}$$

to leading order.

For $r < 0$, or equivalently $p_0 < p_2$, the limit is positive,

$$\lim_{t \to \infty} P_s(t_0, t)|_{r<0} = -\frac{r}{q_2}\left(1 + \frac{Asv}{r^2 + v^2}\right) + \mathcal{O}(A^2), \tag{22}$$

where we have to rely on Eq. (56) being the analytic continuation for the result obtained at positive mass r. Eq. (21) implies that $P_s(t_0, t)$, with or without oscillations, vanishes in the limit of large times as extinction prevails, since $r > 0$. Eq. (22) indicates that the linear increase in $-r$ of the ultimate survival probability is present with or without oscillations, however, that the amplitude of that increase depends on A. As far as the frequency v is concerned, the effect of the oscillations on the ultimate survival is most pronounced for $v = \pm r$,

$$\lim_{t \to \infty} P_s(t_0, t)|_{r<0} = -\frac{r}{q_2} \pm \frac{As}{2q_2} + \mathcal{O}(A^2), \tag{23}$$

with the minimum attained if $v = r$ and the maximum for $v = -r$. It is noteworthy that Eq. (23) no longer vanishes as $r \to 0$. The constraints mentioned above, such as $As \leq r + q_2$, do not affect this result, as $As = q_2/2$ still produces $\lim_{r\to 0^-}\lim_{t\to\infty}P_s(t_0, t)|_{r<0} = 1/4$. Together with Eq. (19) this seems to suggest the possibility of a sudden onset survival, whereby $\lim_{t\to\infty}P_s(t_0, t)$ jumps from 0 at $r = 0$ to a finite value. However, it is crucial in which order limits are taken. Eq. (19) remains valid if $r \to 0$ (tying $v = \pm r$) *before* $t \to \infty$. When taken in this order, the ultimate survival probability is zero at the critical point.

We therefore conclude that the ultimate survival increases linearly and continuously from 0 for $r \geq 0$, Eqs. (19) and (21), to a finite value at $r < 0$, Eq. (22). If the critical point of the present process is defined as the
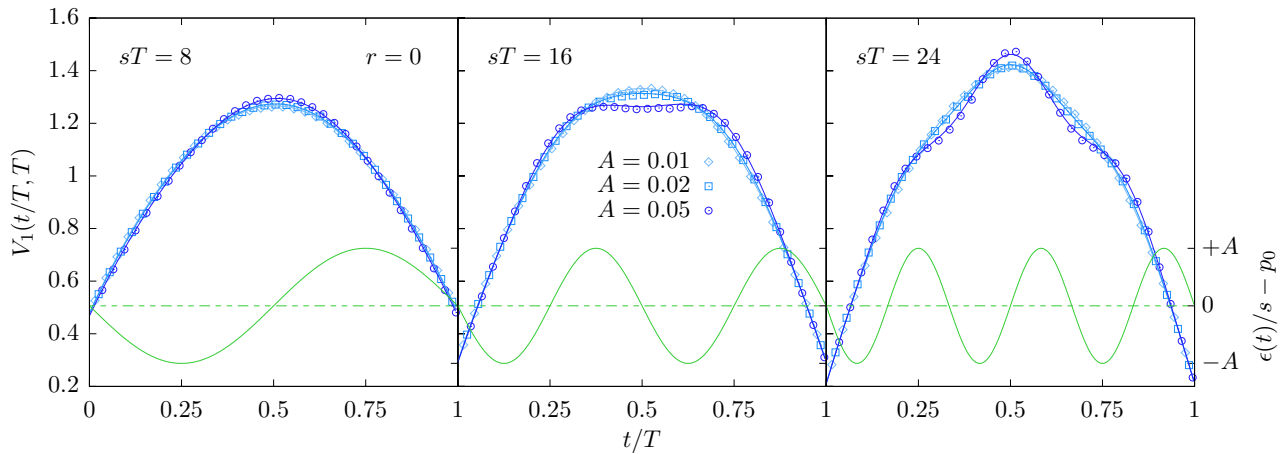
Figure 6. Area-normalised expected avalanche shapes $V_1(t, T)$, Eq. (67), for $r = 0$, $\nu/s = \pi/4$ and $sT \in \{8, 16, 24\}$ for $A \in \{0.01, 0.02, 0.05\}$. The time is rescaled by the termination time T. The system was initialized with one particle at time $t_0 = 0$. Symbols: simulation results obtained by averaging over 10^8 trajectories $N(t)$ with a termination time $sT \pm 0.2$. Full blue lines: analytic prediction to first order in A. Full green lines: perturbation of the extinction rate, Eq. (4) (right ordinate).
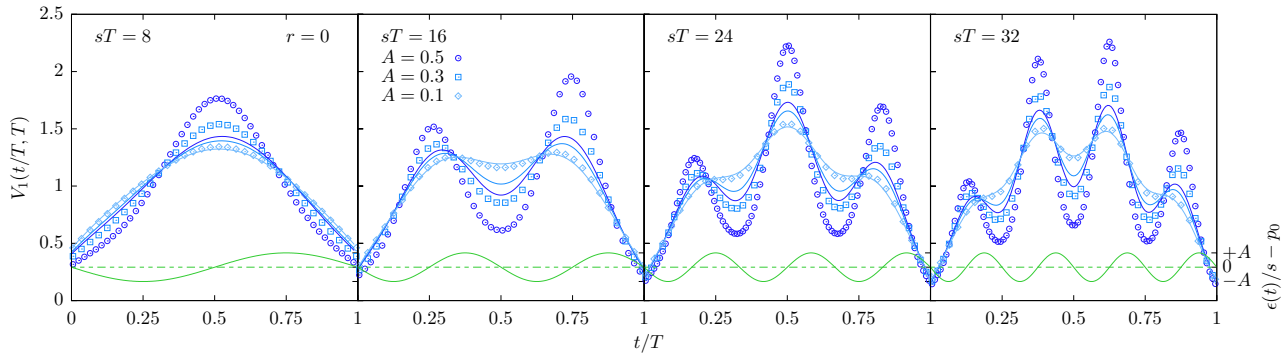
Figure 7. Area-normalised expected avalanche shapes $V_1(t, T)$, Eq. (67), for $r = 0$, $\nu/s = \pi/4$ and $sT \in \{8, 16, 24, 32\}$ for $A \in \{0.1, 0.3, 0.5\}$. The time is rescaled by the termination time T. The system was initialized with one particle at time $t_0 = 0$. Symbols: simulations results obtained by averaging over 10^8 trajectories $N(t)$ with a termination time $sT \pm 0.2$. Full blue lines: analytic prediction to first order in A. Full green lines: perturbation of the extinction rate, Eq. (4) (right ordinate).

onset of ultimate survival, then it is not shifted by the oscillations. Figure 4 shows a comparison of the first-order corrected survival probability Eq. (19) as a function of time to simulation results.

Avalanche shape. *Shape depending on time of death T.* The (temporal) shape of the avalanche $V(t, T)$ is the expectation of $N(t)$ conditioned to the branching process going spontaneously extinct at some fixed termination time $t = T$, *i.e.* for all small $\delta > 0$, $N(T - \delta) > 0$ and $N(T + \delta) = 0$. Typically, time is rescaled to $\tau = t/T$[53].

After suitable normalisation[16] the time-homogeneous version of the process displays a universal, parabolic shape. Not least because of its universality, the shape has gained some popularity to serve as a fingerprint of a process[34,54,55]. However, as shown in Figs. 6 and 7, the periodic extinction imposes characteristic humps on the shape. They are of course rooted in the periodic extinction, as an analytical calculation shows, see "Appendix: Avalanche shape to first order" for details. These oscillations remain visible in the shape $V(t, T)$ at all T and all t, but become particularly vivid whenever the termination time T is commensurate with the period of the oscillations, $2\pi/\nu$. As we have used our field-theoretic scheme only to first order, the slight mismatch with simulation results at larger A, such as those shown in Fig. 7, is not surprising. However, at such large amplitudes, the resulting shape resembles that of recent experimental results, where γ-oscillation modulated the average shape of neuronal avalanches[38]. Furthermore, for larger amplitudes A, the avalanche shapes are asymmetric, which can be seen particularly well in Fig. 7 for $sT = 16$.

Comparison to experiments. The mean avalanche shapes, such as in Figs. 6 and 7 can be qualitatively compared to avalanche profiles recorded in the brain. We reproduce in Fig. 8 plots from Miller et al.[38] (Figure 4(a) in Ref.[38]), and adapt it by overlaying our analytical plots from Fig. 7, in accordance with the Creative Commons Attribu-
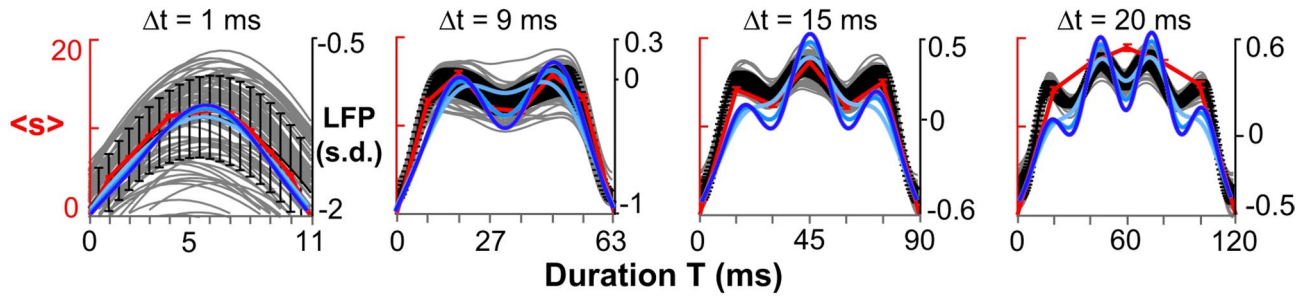
Figure 8. Comparison of model to experimental data. Underlying figure (grey, black and red colors) from Miller et al.[38], Fig. 4(a) therein, reproduced and adapted under Creative Commons Attribution 4.0 International License. Adaptation: overlay of blue colors: analytical results from Fig. 7 above. On y-axis, ⟨s⟩ is the mean profile in Ref.[38], corresponding to our $V(t, T)$; on x-axis, duration T from Ref.[38] is denoted by time t in our article. Data was collected through multielectrode arrays implanted in adult nonhuman primates (see Ref.[38] for details). Grey lines, single electrode data, black line mean of array, red mean size-per-timestep.
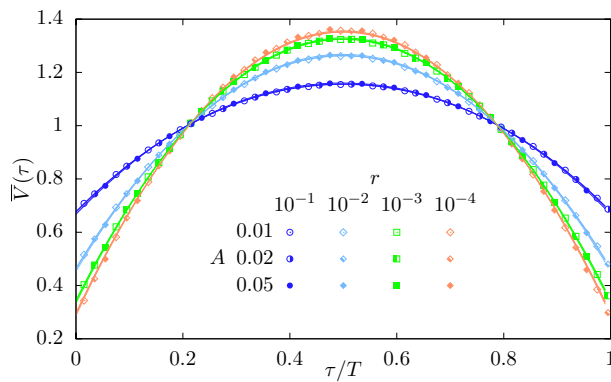
Figure 9. Area-normalized expected avalanche shapes averaged over time of death T, $\overline{V}(\tau)$, Eq. (24), for $r \in \{10^{-4}, 10^{-3}, 10^{-2}, 10^{-1}\}$, $\nu/s = \pi/4$ and $A \in \{0.01, 0.02, 0.05\}$. Before averaging, the time of each avalanche is rescaled by its termination time T. The system was initialized with one particle at time $t_0 = 0$. Symbols: simulations results obtained by averaging over 10^7 trajectories $N(t)$. Full lines: analytic prediction to first order in A.

tion 4.0 International License. The data was collected through multielectrode arrays implanted in three adult nonhuman primates (see Ref.[38] for details).

The plots show qualitatively a good agreement between the data and our model. The general shape and periodicity is captured extremely well. Small qualitative disagreement occurs in the third and fourth plot in the relative heights of consecutive maxima and minima. This disagreement may be down to higher order correction terms in the amplitude A.

The figure illustrates that branching processes, which are commonly used to explain the statistical properties of avalanches recorded in the brain, can be extended to also incorporate neuronal oscillations. Although the observation of non-universal avalanche shapes questioned the criticality hypothesis of the brain[10,32,38], our analytical results clearly show that criticality is compatible with avalanche profiles that are modulated by oscillations.

Universal parabolic shape. The universal parabolic shape may be recovered by suitably averaging across different termination times T. Devising such a scheme in a given numerical or experimental setting may not always be feasible[56]. Figure 9 shows the T-averaged and T-rescaled expected avalanche shape,

$$\overline{V}(\tau) = \frac{\int_0^\infty P_T(T) V(\tau T, T) \mathrm{d}T}{\int_0^1 \int_0^\infty P_T(T) V(\tau T, T) \mathrm{d}T \mathrm{d}\tau}. \tag{24}$$

Varying small amplitudes do not seem to alter this shape and appear to converge to the universal parabola shape when criticality is approached $r \to 0$.

Discussion and conclusion

Our discussion is two-fold: first, we focus on aspects of interest to research in stochastic processes. We then follow with a discussion on the implications for research in the area of neuronal avalanches.

In this paper, we extend the standard branching process by including time-dependent, deterministic variations of a reaction rate. While we focus on varying the extinction rate only, our approach is applicable to any reaction rate in a Doi–Peliti field theory.

Neuronal avalanches can show oscillating behaviour, which we capture with a branching process model with oscillating extinction rate. These oscillations can be observed in any moment, of which we present the zeroth (the survival probability), first and second, and in any correlation function, of which we present the two-time covariance. All of these observables are calculated exactly. Furthermore, we introduce an approximation scheme for factorial moments to first order in the amplitude of the extinction rate oscillations. This allows approximating more complicated observables such as the survival probability and the avalanche shape in the limit of small oscillation amplitudes.

All analytically calculated observables are compared with simulation results from Monte Carlo simulations. While the exact analytic results match perfectly, we also evaluate the first-order approximation scheme and find good agreement in the limit of small oscillation amplitudes.

Although the extinction rate is unchanged on average, its oscillation leads *on average* to a shift in the moments. For example, if the oscillations start with a decrease of the extinction rate, the expected particle number is always greater compared to the process without oscillations. Conversely, if the oscillations start by increasing the extinction rate, the expected number of particles is always lower than without oscillations. Despite the average shift of particle numbers, the onset of indefinite survival is not shifted by the oscillations. We therefore conclude that the critical point remains unchanged.

Both subcritical branching processes and neuronal activity show exponentially decaying auto-correlation functions whose decay rate is independent of the spatial sub-sampling of the neural network[14]. In particular, if the neural system is close to the critical point, in the reverberating regime, the exponential decay is slow and can be observed over more than 100ms even in a single neuron's activity[14]. As the oscillations in the neuronal activity can have periods well below 100 ms (e.g. in the spindle band), they should be visible in the data.

Similarly, both the oscillating branching process presented here and recordings of neuronal avalanches show oscillating avalanche shapes[38]. In our model and in the data, the oscillations modulate the shape and are most pronounced when the avalanche duration is an integer multiple of the period of the oscillations. Surprisingly, these results defy the assumption that the avalanche shape is universal at criticality. However, when the shapes are also rescaled and averaged over the avalanche duration, our simulations indicate that the universal parabola shape is recovered.

In future research, the oscillating branching process should be compared quantitatively to local field potential recordings of oscillating neuronal avalanches. Thus, the presented model can contribute to the understanding of neuronal avalanches by rejecting or supporting the branching process picture of signal propagation in the brain. Furthermore, it would be interesting to find out whether other types of variation of the extinctions rate, such as random fluctuations, result in similar behaviour.

Appendix: Extension of the action

The extension of the model consists of making the extinction rate time-dependent. Hence, in the following derivation, we focus on introducing the new extinction rate and ignore the branching process.

Let $P(n, t)$ be the probability that there are n particles in the system at time t, i.e. $N(t) = n$. Then, the master equation for the extinction process only is

$$\frac{d}{dt}P(n,t) = \epsilon(t)\big((n+1)P(n+1,t) - nP(n,t)\big). \tag{25}$$

The first step in the derivation of the field theory is the introduction of *bra-ket vectors* $\langle n|$ and $|n\rangle$, respectively, and *ladder operators* a and $a^\dagger$. The ket vector $|n\rangle$ represents that there are n particles in the system, while the bra vector $\langle n|$ projects out the state of n particles, $\langle n|m\rangle = \delta_{n,m}$, the Kronecker function. The ladder operator $a^\dagger$ creates an additional particle, $i.e. a^\dagger|n\rangle = |n+1\rangle$, and the operator a annihilates a particle (with the additional prefactor n) $a|n\rangle = n|n-1\rangle$. Thus, the entire, probabilistic state of the system at time t can be represented by a ket vector $|\mathcal{M}(t)\rangle$,

$$|\mathcal{M}(t)\rangle = \sum_{n=0}^{\infty} P(n,t)|n\rangle, \tag{26}$$

which is nothing else than a representation of the probability generating function.

In the next step, following[57], the master Eq. (25) is used to derive a corresponding equation for the state vector $|\mathcal{M}(t)\rangle$,

$$\frac{d}{dt}\Big|\mathcal{M}(t)\Big\rangle = \epsilon(t)\big(a - a^\dagger a\big)\big|\mathcal{M}(t)\big\rangle. \tag{27}$$

In the final step, based on work by Peliti[58], equations such as (27) can be solved by a path integral with an action $\mathcal{A}_\epsilon$, where in every normal-ordered compound operator, a is replaced by a field $\phi(t)$ and $a^\dagger$ is replaced by a field $\phi^\dagger(t)$, and where an additional time-derivative term is added:

$$\mathcal{A}_\epsilon = \int \big(\phi^\dagger(t) - 1\big)\left(-\frac{d}{dt}\phi(t)\right) + \epsilon(t)\big(\phi(t) - \phi^\dagger(t)\phi(t)\big)dt. \tag{28}$$

In general, it is useful to shift the creation field $\phi^\dagger = \widetilde{\phi} + 1$. An explanation of implications of the shift, as well as a more detailed derivation of the path integral can be found in Ref.[59]. Thus, a simpler action is obtained

$$\mathcal{A}_\epsilon = \int \widetilde{\phi}(t)\left(-\frac{\mathrm{d}}{\mathrm{d}t} - \epsilon(t)\right)\phi(t)\mathrm{d}t \,. \tag{29}$$

The total action

$$\mathcal{A} = \int \left\{ \widetilde{\phi}(t)\left(-\frac{\mathrm{d}}{\mathrm{d}t} - \epsilon(t) + sp_2\right)\phi(t) + \sum_{j=2}^{\infty} q_j \widetilde{\phi}^j(t)\phi(t) \right\}\mathrm{d}t \tag{30}$$

enters the path integral in the form $\exp \mathcal{A}$ so that field theoretic expectations become

$$\langle \bullet \rangle = \int \exp(\mathcal{A}) \bullet \mathcal{D}\phi \mathcal{D}\widetilde{\phi} \tag{31}$$

and are calculated by performing the path integral over the bilinear part of the action $\mathcal{A}_0$, Eq. (2), and expanding perturbatively for the term with coupling $sp_0 - \epsilon(t)$, which is unaccounted for in $\mathcal{A}_0$. In connection with the observation of oscillating neuronal avalanches, we choose $\epsilon(t) = sp_0 - As\sin(\nu t)$ and the perturbative part of the action becomes Eq. (5), giving rise to a perturbation theory in small A.

Appendix: Derivation of moments
In order to keep a readable, consistent notation, we use the mathematical notation, e.g. $\mathbb{E}[N(t)]$, when we characterize the statistical properties of $N(t)$. When referring to field-theoretic calculations, we use the notation common in physics, i.e. $\langle \mathcal{O} \rangle$ for the expectation of an observable $\mathcal{O}$. Of course, the two are closely related, e.g. $\langle \phi(t)\phi^\dagger(t_0) \rangle = \mathbb{E}[N(t)|N(t_0) = 1]$ but $\langle \phi^2(t)\phi^\dagger(t_0) \rangle + \langle \phi(t)\phi\phi^\dagger(t_0) \rangle = \mathbb{E}[N^2(t)|N(t_0) = 1]$, Eq. (33). Unless stated otherwise, observables are conditioned to the initialization of the branching process with one particle at time $t_0 = 0$, i.e. $N(0) = 1$, routinely omitted in the mathematical notation. For example, $\mathbb{E}[N(t)]$ is short for $\mathbb{E}[N(t)|N(0) = 1]$.

Appendix: First moment. In the field theoretic calculation, the first moment is calculated as the propagator. Due to the varying extinction rate the propagator acquires corrections which schematically depicted as diagrams. The red, full lines $t_2 \rule{1cm}{0.4pt} t_1$ represent the bare propagator $\langle \phi(t_2)\widetilde{\phi}(t_1) \rangle_0$, while the black dashed lines ending in circles $t' \,\text{--}\text{-}\text{o}$ represent correction terms, where $t_2 \geq t' \geq t_1$. In a Doi–Peliti field theory, these diagrams are by convention read from right to left. The first moment is thus written as follows:

$$\mathbb{E}[N(t)|N(t_0) = 1] = \langle \phi(t)\phi^\dagger(t_0) \rangle = \langle \phi(t)\widetilde{\phi}(t_0) \rangle \,\hat{=}\, \rule{1cm}{0.4pt} + \rule{1cm}{0.4pt}\text{o} + \rule{1cm}{0.4pt}\text{o}\rule{0.5cm}{0.4pt}\text{o} + \dots \tag{32a}$$

$$= \Theta(t)e^{-rt}\left(1 + \int_{t_0}^{t} sA\sin(\nu t')\mathrm{d}t' + \int_{t_0}^{t} sA\sin(\nu t')\int_{t_0}^{t'} sA\sin(\nu t'')\mathrm{d}t''\mathrm{d}t' + \dots\right)$$

$$= \Theta(t)e^{-rt}\left(\sum_{\ell=0}^{\infty} \frac{1}{\ell!}\int_{t_0}^{t} sA\sin(\nu t')\mathrm{d}t'\right) \tag{32b}$$

$$= \Theta(t)\exp\left(-r + \int_{t_0}^{t} sA\sin(\nu t')\mathrm{d}t'\right),$$

exactly as expected for an inhomogeneous Poisson process with time-varying intensity that governs the extinction[51]. For $t_0 = 0$, this reproduces the result for $\mathbb{E}[N(t)]$, Eq. (6).

Appendix: Second moment. The second moment $\mathbb{E}[N^2(t)]$ is determined field-theoretically on the basis of the square of the particle number operator, $(a^\dagger a)^2 = (a^\dagger)^2 a^2 + a^\dagger a$, which is easily expressed in terms of fields $\phi^\dagger$ and ϕ once in normal-ordered form,

$$\mathbb{E}[N^2(t)] = \langle \phi^2(t)\widetilde{\phi}(0) \rangle + \underbrace{\langle \phi(t)\widetilde{\phi}(0) \rangle}_{=\mathbb{E}[N(t)]} \,. \tag{33}$$

Diagrammatically, the first term is

$$\langle \phi^2(t)\widetilde{\phi}(0) \rangle \,\hat{=}\, \rule{1cm}{0.4pt} \tag{34}$$

which is a convolution in direct time,

$$\langle \phi^2(t)\widetilde{\phi}(0)\rangle = 2q_2 \int\limits_0^t \left\langle \phi(t)\widetilde{\phi}(t')\right\rangle^2 \left\langle \phi(t')\widetilde{\phi}(0)\right\rangle \mathrm{d}t', \tag{35}$$

that can be calculated with the help of Eq. (32b) to produce Eq. (7).

Appendix: n-th factorial moment to first order.

We define the n-th factorial moment of $N(t)$[16] as the function

$$g_n(t_0, t) = \left\langle \phi(t)^n \widetilde{\phi}(t_0)\right\rangle = g_n^{(0)}(t_0, t) + A g_n^{(1)}(t_0, t) + A^2 g_n^{(2)}(t_0, t) + \cdots \tag{36}$$

where the additional extinction $-A\sin(\nu t)$, Eq. (4), is dealt with perturbatively about $A = 0$. The zeroth-order correction $g_n^{(0)}(t_0, t)$ corresponds to the sum of binary tree diagrams with one in-coming leg and n out-going legs. Since the zeroth-order correction does not include any perturbation in the extinction rate, the process is homogeneous in time and, therefore, it does not depend on the initial time t_0, but rather on the amount of time $t - t_0$.

In Ref.[16], the function $g_n^{(0)}(t_0, t)$ was derived from the following forest (meaning it contains a sum of tree-like diagrams)

$$g_n^{(0)}(t_0,t) \mathrel{\hat=} \sum_{\ell=1}^n \sum_{m_1,\ldots,m_\ell=1}^n \binom{n}{m_1,\ldots,m_\ell} \quad \mathrel{\hat=} n! e^{-r(t-t_0)}\left(\frac{q_2}{r}\left(1 - e^{-r(t-t_0)}\right)\right)^{n-1}.$$

$$\tag{37}$$

This zeroth-order correction satisfies the identity

$$g_n^{(0)}(t_0,t) = \sum_{\ell=1}^n g_\ell^{(0)}(t',t)\frac{1}{\ell!}\sum_{m_1,\ldots,m_\ell=1}^n \binom{n}{m_1,\ldots,m_\ell} g_{m_1}^{(0)}(t_0,t')\cdots g_{m_\ell}^{(0)}(t_0,t'), \tag{38}$$

which can be obtained by choosing an arbitrary time $t' \in [t_0, t]$ when a diagram has ℓ legs, *cf.* Eq. (40a), and reconstructing the entire forest. As the left-hand side of Eq. (38) does not depend on t' it might be tempting to differentiate with respect to t', but for our purposes the sum

$$\frac{\partial}{\partial t}g_n^{(0)}(t_0,t) = \sum_{\ell=1}^n \frac{\partial}{\partial t}g_\ell^{(0)}(t',t)\frac{1}{\ell!}\sum_{m_1,\ldots,m_\ell=1}^n \binom{n}{m_1,\ldots,m_\ell} g_{m_1}^{(0)}(t_0,t')\cdots g_{m_\ell}^{(0)}(t_0,t') \tag{39}$$

will prove particularly useful.

We proceed with the construction of the first order correction $A g_n^{(1)}(t)$ of $g_n(t)$. This correction contains the external perturbation $\mathrm{d}t' A s \sin(\nu t')$ once in each diagram. It needs to be attached to every tree diagram at time t', as indicated by the vertical dotted line in the diagram below,

$$g_n^{(1)}(t_0,t) \mathrel{\hat=} \int_{t_0}^t \sum_{\ell=1}^n \sum_{m_1,\ldots,m_\ell}^n \binom{n}{m_1,\ldots,m_\ell} \quad \mathrm{d}t' \tag{40a}$$

$$= s\int_{t_0}^t \sin(\nu t')\sum_{\ell=1}^n \ell g_\ell^{(0)}(t_0,t')\frac{1}{\ell!}\sum_{m_1,\ldots,m_\ell=1}^n \binom{n}{m_1,\ldots,m_\ell} g_{m_1}^{(0)}(t',t)\cdots g_{m_\ell}^{(0)}(t',t)\, \mathrm{d}t'$$

$$= s\int_0^{t-t_0} \sin(\nu(t-t'))\sum_{\ell=1}^n \ell g_\ell^{(0)}(0,t-t_0-t'')\frac{1}{\ell!}\sum_{m_1,\ldots,m_\ell=1}^n \binom{n}{m_1,\ldots,m_\ell} g_{m_1}^{(0)}(0,t'')\cdots g_{m_\ell}^{(0)}(0,t'')\, \mathrm{d}t'', \tag{40b}$$

where the last identity is obtained by the substitution $t'' = t - t'$ and using the time-homogeneity $g_\ell^{(0)}(t_0,t) = g_\ell^{(0)}(0, t-t_0)$. Defining the sum

$$S(t-t_0, t'') = \sum_{\ell=1}^n \ell g_\ell^{(0)}(0,t-t_0-t'')\frac{1}{\ell!}\sum_{m_1,\ldots,m_\ell=1}^n \binom{n}{m_1,\ldots,m_\ell} g_{m_1}^{(0)}(0,t'')\cdots g_{m_\ell}^{(0)}(0,t''), \tag{41}$$

the first order perturbation can be written as

$$g_n^{(1)}(t_0, t) = s \int_0^{t-t_0} \sin(\nu(t - t'))S(t - t_0, t'')dt'' .$$ (42)

The sum $S(t - t_0, t'')$, Eq. (41), would be equal to $g_n^{(0)}(t_0, t)$, Eq. (38), was it not for the factor ℓ in front of $g_\ell^{(0)}(0, t - t_0 - t'')$, corresponding to the ℓ legs at time t' to choose from to insert the external perturbation. Nevertheless, the summation Eq. (41) can be carried out by using $g_n^{(0)}$ of Eq. (37) as a generating function. The term $\ell g_\ell^{(0)}(t_0, t)$ can be obtained from the time-derivative of the function $g_n^{(0)}(t_0, t)$ in Eq. (37),

$$\frac{\partial}{\partial t}g_\ell^{(0)}(t_0, t) = rg_\ell^{(0)}(t_0, t)\frac{\ell e^{-r(t-t_0)} - 1}{1 - e^{-r(t-t_0)}} ,$$ (43)

which produces the identity

$$\ell g_\ell^{(0)}(t_0, t) = \exp r(t - t_0)\left(g_\ell^{(0)}(t_0, t) + \frac{1}{r}\left(1 - \exp -r(t - t_0)\right)\frac{\partial}{\partial t}g_\ell^{(0)}(t_0, t)\right).$$ (44)

Rewriting $\ell g_\ell^{(0)}(0, t - t_0 - t'') = \ell g_\ell^{(0)}(t_0 + t'', t)$ in Eq. (41) in terms of $\frac{\partial}{\partial t}g_\ell^{(0)}(t_0, t)$ and multiples of $g_\ell^{(0)}(t_0, t)$ according to Eq. (44) allows the summation to be carried out, using Eqs. (38) and (39), which eventually gives

$$S(t - t_0, t'') = g_n^{(0)}(0, t - t_0)\left(1 + (n - 1)\frac{e^{-rt''} - e^{-r(t-t_0)}}{1 - e^{-r(t-t_0)}}\right),$$ (45)

and therefore Eq. (12). For what follows, this is best re-written as

$$g_n^{(1)}(t_0, t) = g_n^{(0)}(t_0, t)\left(u(t_0, t) + (n - 1)v(t_0, t)\right)$$ (46)

with

$$u(t_0, t) = s\int_0^{t-t_0}\sin(\nu(t - t'))dt' = \frac{s}{\nu}(\cos(\nu t_0) - \cos(\nu t))$$ (47a)

$$\begin{aligned} v(t_0, t) &= s\int_0^{t-t_0}\sin(\nu(t - t'))\frac{e^{-rt'} - e^{-r(t-t_0)}}{1 - e^{-r(t-t_0)}}dt' \\ &= \frac{s}{1 - e^{-r(t-t_0)}}\left[\frac{1}{\nu}\exp -r(t - t_0)(\cos(\nu t) - \cos(\nu t_0)) \right. \\ &\quad \left. + \frac{1}{r^2 + \nu^2}\left(r\sin(\nu t) - \nu\cos(\nu t) + \exp -r(t - t_0)(\nu\cos(\nu t_0) - r\sin(\nu t_0))\right)\right]. \end{aligned}$$ (47b)

Appendix: Further observables

Appendix: Covariance. The covariance is defined as

$$\text{Cov}(N(t_1), N(t_2)) = \mathbb{E}[N(t_1)N(t_2)] - \mathbb{E}[N(t_1)]\mathbb{E}[N(t_2)],$$ (48)

where all expectations are conditioned to $N(0) = 1$. In the field theory, the term $\mathbb{E}[N(t_1)N(t_2)]$ is calculated as

$$\mathbb{E}[N(t_1)N(t_2)] = \langle\phi(t_{\max})\phi^\dagger(t_{\min})\phi(t_{\min})\phi^\dagger(0)\rangle = \langle\phi(t_{\max})\phi(t_{\min})\widetilde{\phi}(0)\rangle + \langle\phi(t_{\max})\widetilde{\phi}(t_{\min})\phi(t_{\min})\widetilde{\phi}(0)\rangle,$$ (49)

where $t_{\max} = \max\{t_1, t_2\}$ and $t_{\min} = \min\{t_1, t_2\}$. The first term of Eq. (49) is a convolution similar to Eqs. (34) and (35),

$$\left\langle\phi(t_{\max})\phi(t_{\min})\widetilde{\phi}(0)\right\rangle \hat{=} \quad \underset{t_{\min}}{\overset{t_{\max}}{\rangle}} \!-\! 0 \quad \hat{=} 2q_2\int\left\langle\phi(t_{\max})\widetilde{\phi}(t')\right\rangle\left\langle\phi(t_{\min})\widetilde{\phi}(t')\right\rangle\left\langle\phi(t')\widetilde{\phi}(0)\right\rangle dt',$$ (50)

while the second term is a product of two first moments,

$$\left\langle\phi(t_{\max})\widetilde{\phi}(t_{\min})\phi(t_{\min})\widetilde{\phi}(0)\right\rangle \hat{=} \overset{t_{\max}\quad t_{\min}\quad 0}{\rule{2cm}{0.4pt}\;\rule{1cm}{0.4pt}} \hat{=} \left\langle\phi(t_{\max})\widetilde{\phi}(t_{\min})\right\rangle\left\langle\phi(t_{\min})\widetilde{\phi}(0)\right\rangle.$$ (51)

At $t_1 = t_2$, when $\left\langle\phi(t_{\max})\widetilde{\phi}(t_{\min})\right\rangle = 1$, Eq. (49) recovers Eq. (33).

Appendix: Probability of survival to first order. The survival probability $P_s(t_0, t)$ is determined via the probability $P(N(t) = 0|N(t_0) = 1) = 1 - P_s(t_0, t)$ that the system contains no particles at time t. Field-theoretically that is $\left\langle\exp -\phi(t)\phi^\dagger(t_0)\right\rangle^{16, 59}$ so that

$$P_s(t_0, t) = 1 - \left\langle \exp -\phi(t)\phi^\dagger(t_0) \right\rangle = - \sum_{n=1}^{\infty} \frac{(-)^n}{n!} \left\langle \phi^n(t)\widetilde{\phi}(t_0) \right\rangle = \sum_{n=1}^{\infty} \frac{(-)^{n-1}}{n!} g_n(t_0, t) \,. \tag{52}$$

To zeroth order the summation is easily carried out, since $g_n^{(0)}(t_0, t)$, Eq. (37), may be written as $g_n(t_0, t) = n!\alpha\beta^{n-1}$ with $\alpha = \exp -r(t - t_0)$ and $\beta = q_2(1 - \exp -r(t - t_0))/r$,

$$P_s(t_0, t) = \alpha \sum_{m=0}^{\infty} (-\beta)^m + \mathcal{O}(A) = \frac{\alpha}{1 + \beta} + \mathcal{O}(A) \,, \tag{53}$$

as shown in Eq. (42) in Ref.[16]. Using the first-order corrected $g_n(t_0, t)$, Eq. (46), the summation does not change significantly as far as the term $Au(t_0, t)$ is concerned, but $A(n-1)v(t_0, t)$ requires some additional work. Recognising that Eq. (53) is effectively a generating function, the required sum is easily obtained from Eq. (53),

$$P_s(t_0, t) = \frac{\alpha}{1 + \beta}(1 + Au(t_0, t)) + \beta \frac{\partial}{\partial \beta} \frac{\alpha}{1 + \beta} Av(t_0, t) \tag{54}$$

To reduce clutter, we expand $u(t_0, t)$ and $v(t_0, t)$ only for the specific case of $t_0 = 0$. Using

$$P_s^{(0)}(0, t) = \frac{\exp -rt}{1 + \frac{q_2}{r}(1 - \exp -rt)} \tag{55}$$

for the zeroth order approximation, the survival probability to first order reads

$$
\begin{aligned}
P_s(0, t) = P_s^{(0)}(0, t) \Bigg\{ 1 + As \Bigg[& \frac{1}{v} + P_s^{(0)}(0, t)\frac{q_2 r}{(r^2 + v^2)v} \\
& - \cos(vt)\left(\frac{1}{v} + P_s^{(0)}(0, t)\frac{q_2}{r}\left(\frac{1}{v} - \frac{v}{\exp -rt(r^2 + v^2)} \right) \right) \\
& - \sin(vt)\left(P_s^{(0)}(0, t)\frac{q_2}{\exp -rt(r^2 + v^2)} \right) \Bigg] \Bigg\} + \mathcal{O}(A^2) \,.
\end{aligned}
\tag{56}
$$

Appendix: Avalanche shape to first order. In Refs.[16, 59], it is shown that the avalanche shape (temporal profile) of a branching process can be related to the incompletely normalised average

$$\mathbb{E}[N(t); N(T) = 0 | N(t_0) = 1] = \sum_N N P(N(t) = N, N(T) = 0 | N(t_0) = 1) \,, \tag{57}$$

which is the average population size N at time t taken over the joint probability $P(N(t) = N, N(T) = 0 | N(t_0) = 1)$ of having size N at time t and size 0 at time T, conditioned to having size 1 at time t_0. This quantity is easily captured in the field theory,

$$
\begin{aligned}
\mathbb{E}[N(t); N(T) = 0 | N(t_0) = 1] &= \left\langle \exp -\phi(T)\phi^\dagger(t)\phi(t)\phi^\dagger(t_0) \right\rangle \\
&= \left\langle \phi(t)\widetilde{\phi}(t_0) \right\rangle + \sum_{n=1}^{\infty} \frac{(-1)^n}{n!}\left(\left\langle \phi^n(T)\phi(t)\widetilde{\phi}(t_0) \right\rangle + \left\langle \phi^n(T)\widetilde{\phi}(t)\phi(t)\widetilde{\phi}(t_0) \right\rangle \right).
\end{aligned}
\tag{58}
$$

Using identities (B2) and (B3) of Ref.[16] in the form

$$\left\langle \phi^n(T)\phi(t)\widetilde{\phi}(t_0) \right\rangle = \sum_{k=1}^{n} \sum_{m_1,\ldots,m_k=1}^{n} \binom{n}{m_1,\ldots,m_k} g_{m_1}(t, T)\ldots g_{m_k}(t, T)g_{k+1}(t_0, t)\frac{1}{k!} \tag{59}$$

and

$$\left\langle \phi^n(T)\widetilde{\phi}(t)\phi(t)\widetilde{\phi}(t_0) \right\rangle = \sum_{k=1}^{n} \sum_{m_1,\ldots,m_k=1}^{n} \binom{n}{m_1,\ldots,m_k} g_{m_1}(t, T)\ldots g_{m_k}(t, T)g_k(t_0, t)\frac{1}{(k-1)!} \,, \tag{60}$$

and writing $g_n(t_0, t) = n!\alpha\beta^{n-1}$ and $g_n(t, T) = n!ab^{n-1}$, Eq. (58) can be written at $A = 0$ after some tedious algebra

$$\mathcal{S} := \mathbb{E}[N(t); N(T) = 0 | N(t_0) = 1]\alpha - \frac{a\alpha}{1 + b\left(1 + \frac{a\beta}{b}\right)}\left[1 + \beta\left(2 - \frac{a(1 + \beta)}{1 + b\left(1 + \frac{a\beta}{b}\right)} \right) \right]. \tag{61}$$

To zeroth order in A, we recover the result in Ref.[16] with $\alpha = \exp -r(t - t_0)$, $\beta = \frac{q_2}{r}(1 - \exp -r(t - t_0))$, as used in "Probability of survival to first order", as well as $a = \exp -r(T - t)$ and $b = \frac{q_2}{r}(1 - \exp -r(T - t))$. To incorporate the first-order correction, we adjust α, β, a and b so that $g_n(t_0, t)$ and $\langle N(t), N(t_0) = 1, N(T) = 0 \rangle$ can be calculated order by order via generating functions. Defining

$$\alpha = \exp -r(t - t_0)(1 + A_1), \tag{62a}$$

$$\beta = \frac{q_2}{r}\big(1 - \exp -r(t - t_0)\big)z_1, \tag{62b}$$

$$a = \exp -r(T - t)(1 + A_2), \tag{62c}$$

$$b = \frac{q_2}{r}\big(1 - \exp -r(T - t)\big)z_2, \tag{62d}$$

and the generating function $\mathcal{G} = n!\alpha\beta^{n-1}$, we recover $g_n(t_0, t)$ to first order according to Eq. (46) in the form

$$g_n(t_0, t) = \left\{\mathcal{G} + A\Big(u(t_0, t)\frac{\partial \mathcal{G}}{\partial A_1} + v(t_0, t)\frac{\partial \mathcal{G}}{\partial z_1}\Big)\right\}\Big|_{A_1 = 0, z_1 = 1} + \mathcal{O}\big(A^2\big), \tag{63}$$

and using the generating function $\mathcal{S}$ as defined in Eq. (61), similarly for the avalanche shape,

$$\mathbb{E}[N(t); N(T) = 0 | N(t_0) = 1]$$
$$= \left\{\mathcal{S} + A\Big(u(t_0, t)\frac{\partial \mathcal{S}}{\partial A_1} + u(t, T)\frac{\partial \mathcal{S}}{\partial A_2} + v(t_0, t)\frac{\partial \mathcal{S}}{\partial z_1} + v(t, T)\frac{\partial \mathcal{S}}{\partial z_2}\Big)\right\}\Big|_{A_1 = 0, z_1 = 1, A_2 = 0, z_2 = 1} + \mathcal{O}\big(A^2\big). \tag{64}$$

At this point, it is worth noting that Eq. (64) is a general expression whose dependence on the time-dependent extinction rate lies in the functions u and v. Hence, this expression of the avalanche shape holds for different time-dependent extinction rates as long as u and v are calculated along the lines of Eq. (47) As indicated earlier, the expression in Eq. (64) is the expectation of N over the *joint* probability of $N(t) = N$ and $N(T) = 0$. This includes all trajectories that become extinct before time T. To calculate the avalanche shape of those instances that become extinct exactly at time T, we need the expectation of $N(t)$ *conditioned* to $N(T) = 0$ and $N(t) > 0$ for $t < T$,

$$V(t, T) = \mathbb{E}[N(t) | N(T > t > t_0) > 0, N(T) = 0, N(t_0) = 1]. \tag{65}$$

Assuming $dT > 0$, those trajectories that have $N(T + dT) = 0$ but $N(T) \neq 0$, have the desired feature of going extinct precisely at time T. Since $N(T) = 0$ implies $N(T + dT) = 0$, the shape $V(t, T)$ is equal to the expectation $\mathbb{E}[N(t); N(T) = 0 | N(t_0) = 1]$ differentiated with respect to T, and normalised by the probability density of extinction at exactly time T,

$$V(t, T) = \frac{\frac{d}{dT}\mathbb{E}[N(t); N(T) = 0 | N(t_0) = 1]}{-\frac{d}{dT}P_s(0, T)}, \tag{66}$$

which can be calculated to first order in A by using Eqs. (56) and (64). However, numerically it is much easier to normalise the avalanche shape $V(t, T)$ by the area under its curve

$$V_1(t, T) = \frac{V(t, T)}{\int_0^1 V(\tau T, T)d\tau}, \tag{67}$$

which is what is shown in the plots in Figs. 6 and 7.

References

1. Dayan, P. & Abbott, L. *Theoretical Neuroscience* (The MIT Press, Cambridge, 2001).
2. Plenz, D. & Aertsen, A. Neural dynamics in cortex-striatum co-cultures—I. Anatomy and electrophysiology of neuronal cell types. *Neuroscience* **70**, 861–891. https://doi.org/10.1016/0306-4522(95)00406-8 (1996).
3. Plenz, D. & Kitai, S. T. Up and down states in striatal medium spiny neurons simultaneously recorded with spontaneous activity in fast-spiking interneurons studied in cortex–striatum–substantia nigra organotypic cultures. *J. Neurosci.* **18**, 266–283. https://doi.org/10.1523/JNEUROSCI.18-01-00266.1998 (1998).
4. Karpiak, V. C. & Plenz, D. Preparation and maintenance of organotypic cultures for multi-electrode array recordings. *Curr. Protoc. Neurosci.* **19**, 6.15.1-6.15.8. https://doi.org/10.1002/0471142301.ns0615s19 (2002).
5. Beggs, J. M. & Plenz, D. Neuronal avalanches in neocortical circuits. *J. Neurosci.* **23**, 11167–11177 (2003).
6. Beggs, J. M. & Plenz, D. Neuronal avalanches are diverse and precise activity patterns that are stable for many hours in cortical slice cultures. *J. Neurosci.* **24**, 5216–5229 (2004).
7. Priesemann, V., Munk, M. H. & Wibral, M. Subsampling effects in neuronal avalanche distributions recorded in vivo. *BMC Neurosci.* **10**, 1–20. https://doi.org/10.1186/1471-2202-10-40 (2009).
8. Priesemann, V., Valderrama, M., Wibral, M. & Quyen, M. L. V. Neuronal avalanches differ from wakefulness to deep sleep–evidence from intracranial depth recordings. *PLoS Comput. Biol.* https://doi.org/10.1371/journal.pcbi.1002985 (2013).
9. Wagenaar, D. A., Pine, J. & Potter, S. M. An extremely rich repertoire of bursting patterns during the development of cortical cultures. *BMC Neurosci.* **7**, 11. https://doi.org/10.1186/1471-2202-7-11 (2006).
10. Beggs, J. M. The criticality hypothesis: How local cortical networks might optimize information processing. *Philos. Trans. R. Soc. A* **366**, 329–343 (2008).

11. Brochini, L. *et al.* Phase transitions and self-organized criticality in networks of stochastic spiking neurons. *Sci. Rep.* https://doi.org/10.1038/srep35831 (2016).

12. Haldeman, C. & Beggs, J. M. Critical branching captures activity in living neural networks and maximizes the number of metastable states. *Phys. Rev. Lett.* **94**, 058101. https://doi.org/10.1103/PhysRevLett.94.058101 (2005).

13. Williams-García, R. V., Moore, M., Beggs, J. M. & Ortiz, G. Quasicritical brain dynamics on a nonequilibrium widom line. *Phys. Rev. E* **90**, 062714. https://doi.org/10.1103/PhysRevE.90.062714 (2014).

14. Wilting, J. & Priesemann, V. Between perfectly critical and fully irregular: A reverberating model captures and predicts cortical spike propagation. *Cereb. Cortex* **29**, 2759–2770. https://doi.org/10.1093/cercor/bhz049 (2019).

15. Pruessner, G. *Self-Organised Criticality* (Cambridge University Press, Cambridge, 2012).

16. Garcia-Millan, R., Pausch, J., Walter, B. & Pruessner, G. Field-theoretic approach to the universality of branching processes. *Phys. Rev. E* **98**, 062107. https://doi.org/10.1103/PhysRevE.98.062107 (2018).

17. Watson, H. & Galton, F. On the probability of the extinction of families. *R. Anthropol. Inst. G. B. Irel.* **4**, 138–144 (1875).

18. Harris, T. E. *The Theory of Branching Processes* (Springer, Berlin, 1963).

19. Athreya, K. B. & Ney, P. E. *Branching processes, vol. 196 of Grundlehren der mathematischen Wissenschaften* (Springer, Berlin, 1972).

20. Pázsit, I. & Pál, L. *Neutron Fluctuations: A Treatise on the Physics of Branching Processes* (Elsevier, Amsterdam, 2007).

21. Williams, M. *Random Processes in Nuclear Reactors* (Elsevier, Amsterdam, 2013).

22. Marzocchi, W. & Lombardi, A. A double branching model for earthquake occurrence. *J. Geophys. Res.* https://doi.org/10.1029/2007JB005472 (2008).

23. Lee, D., Goh, K.-I., Kahng, B. & Kim, D. Branching process approach to avalanche dynamics on complex networks. *J. Korean Phys. Soc.* **44**, 633–637 (2004).

24. Simkin, M. & Roychowdhury, V. Re-inventing willis. *Phys. Rep.* **502**, 1–35. https://doi.org/10.1016/j.physrep.2010.12.004 (2010).

25. Durrett, R. Branching process models of cancer. In *Branching Process Models of Cancer* 1–63 (Springer, Berlin, 2015).

26. Gleeson, J. P. & Durrett, R. Temporal profiles of avalanches on networks. *Nat. Commun.* **8**, 1227 (2017).

27. Seshadri, S., Klaus, A., Winkowski, D. E., Kanold, P. O. & Plenz, D. Altered avalanche dynamics in a developmental nmdar hypofunction model of cognitive impairment. *Transl. Psychiatry* **8**, 3 (2018).

28. Poil, S.-S., can Ooyen, A. & Linkenkaer-Hansen, K. Avalanche dynamics of human brain oscillations: Relation to critical branching process and temporal correlations. *Hum. Brain Mapp.* **29**, 770–777. https://doi.org/10.1002/hbm.20590 (2008).

29. Wilting, J. *et al.* Operating in a reverberating regime enables rapid tuning of network states to task requirements. *Front. Syst. Neurosci.* https://doi.org/10.3389/fnsys.2018.00055 (2018).

30. Wilting, J. & Priesemann, V. Inferring collective dynamical states from widely unobserved systems. *Nat. Commun.* **9**, 2325. https://doi.org/10.1038/s41467-018-04725-4 (2018).

31. Timme, N. M. *et al.* Criticality maximizes complexity in neural tissue. *Front. Physiol.* **7**, 425. https://doi.org/10.3389/fphys.2016.00425 (2016).

32. Wilting, J. & Priesemann, V. 25 years of criticality in neuroscience: Established results, open controversies, novel concepts. *Curr. Opin. Neurobiol.* **58**, 105–111. https://doi.org/10.1016/j.conb.2019.08.002 (2019).

33. Goldstein, M. L., Morris, S. A. & Yen, G. G. Problems with fitting to the power-law distribution. *Eur. Phys. J. B Condens. Matter Complex Syst.* **41**, 255–258. https://doi.org/10.1140/epjb/e2004-00316-5 (2004).

34. Papanikolaou, S. *et al.* Universality beyond power laws and the average avalanche shape. *Nat. Phys.* **7**, 316–320. https://doi.org/10.1038/nphys1884 (2011).

35. Friedman, N. *et al.* Universal critical dynamics in high resolution neuronal avalanche data. *Phys. Rev. Lett.* **108**, 208102. https://doi.org/10.1103/PhysRevLett.108.208102 (2012).

36. Laurson, L. *et al.* Evolution of the average avalanche shape with the universality class. *Nat. Commun.* **4**, 2927. https://doi.org/10.1038/ncomms3927 (2013).

37. Rybarsch, M. & Bornholdt, S. Avalanches in self-organized critical neural networks: A minimal model for the neural soc universality class. *PLoS One* https://doi.org/10.1371/journal.pone.0093090 (2014).

38. Miller, S. R., Yu, S. & Plenz, D. The scale-invariant, temporal profile of neuronal avalanches in relation to cortical γ-oscillations. *Sci. Rep.* https://doi.org/10.1038/s41598-019-52326-y (2019).

39. Berger, H. über das elektrenkephalogramm des menschen. *Arch. Psychiatr.* **87**, 527–570. https://doi.org/10.1007/BF01797193 (1929).

40. Buzsáki, G. & Draguhn, A. Neuronal oscillations in cortical networks. *Science* **304**, 1926–1929. https://doi.org/10.1126/science.1099745 (2004).

41. Penttonen, M. & Buzsáki, G. Natural logarithmic relationship between brain oscillators. *Thalamus Relat. Syst.* **2**, 145–152. https://doi.org/10.1017/S1472928803000074 (2003).

42. Lombardi, F., Herrmann, H. J., Plenz, D. & DeArcangelis, L. On the temporal organization of neuronal avalanches. *Front. Syst. Neurosci.* **8**, 1–15. https://doi.org/10.3389/fnsys.2014.00204 (2014).

43. Engel, A. K. & Fries, P. Beta-band oscillations—signalling the status quo. *Curr. Opin. Neurobiol.* **20**, 156–165. https://doi.org/10.1016/j.conb.2010.02.015 (2010).

44. Lundqvist, M., Herman, P. & Lansner, A. Theta and gamma power increases and alpha/beta power decreases with memory load in an attractor network model. *J. Cogn. Neurosci.* **23**, 3008–3020. https://doi.org/10.1162/jocn_a_00029 (2011).

45. Lisman, J. E. & Jensen, O. The theta-gamma neural code. *Neuron* **77**, 1002–1016. https://doi.org/10.1016/j.neuron.2013.03.007 (2013).

46. Buzsáki, G., Logothetis, N. & Singer, W. Scaling brain size, keeping timing: Evolutionary preservation of brain rythms. *Neuron* **80**, 751–764. https://doi.org/10.1016/j.neuron.2013.10.002 (2013).

47. Lundqvist, M. *et al.* Gamma and beta bursts underlie working memory. *Neuron* **90**, 152–164. https://doi.org/10.1016/j.neuron.2016.02.028 (2016).

48. Iemi, L. *et al.* Multiple mechanisms link prestimulus neural oscillations to sensory responses. *eLife* **8**, 1–34. https://doi.org/10.7554/eLife.43620 (2019).

49. Lombardi, F., Herrmann, H., Perrone-Capano, C., Plenz, D. & DeArcangelis, L. Balance between excitation and inhibition controls the temporal organization of neuronal avalanches. *Phys. Rev. Lett.* **108**, 1–5. https://doi.org/10.1103/PhysRevLett.108.228703 (2012).

50. Nikolić, D., Fries, P. & Singer, W. Gamma oscillations: Precise temporal coordination without a metronome. *Trends Cogn. Sci.* **17**, 54–55. https://doi.org/10.1016/j.tics.2012.12.003 (2013).

51. Kingman, J. *Poisson Processes* (Clarendon Press, Oxford, 1992).

52. Park, K. I *Fundamentals of Probability and Stochastic Processes with Applications to Communications* (Springer, New York, 2018).

53. Kuntz, M. C. & Sethna, J. P. Noise in disordered systems: The power spectrum and dynamic exponents in avalanche models. *Phys. Rev. B* **62**, 11699–11708. https://doi.org/10.1103/PhysRevB.62.11699 (2000).

54. Dobrinevski, A., Doussal, P. L. & Wiese, K. J. Avalanche shape and exponents beyond mean-field theory. *Europhys. Lett.* **108**, 66002 (2014).

55. Baldassarri, A., Colaiori, F. & Castellano, C. Average shape of a fluctuation: Universality in excursions of stochastic processes. *Phys. Rev. Lett.* **90**, 060601 (2003).

56. Willis, G. & Pruessner, G. Spatio-temporal correlations in the manna model in one, three and five dimensions. *Int. J. Mod. Phys.* **32**, 1830002 (2018).
57. Doi, M. Second quantization representation for classical many-particle system. *J. Phys. A Math. Gen.* **9**, 1465–1477 (1976).
58. Peliti, L. Path integral approach to birth-death processes on a lattice. *J. Phys. (Paris)* **46**, 1469–1483 (1985).
59. Pausch, J. *Topics in Statistical Mechanics*. Ph.D. thesis, Imperial College London (2019). http://dl.handle.net/10044/1/73905.

Acknowledgements

Author contributions

All authors contributed equally.

Competing interests

The authors declare no competing interests.

Additional information

Correspondence and requests for materials should be addressed to J.P.

Reprints and permissions information is available at www.nature.com/reprints.

Publisher's note Springer Nature remains neutral with regard to jurisdictional claims in published maps and institutional affiliations.